EDGE ARTICLE

Check for updates

An N-heterocyclic carbene ligand promotes highly selective alkyne semihydrogenation with copper nanoparticles supported on passivated silica†

Nicolas Kaeffer, [ID] Hsueh-Ju Liu, [ID] ‡ Hung-Kun Lo, Alexey Fedorov [ID] * and Christophe Copéret [ID] *

We report a surface organometallic route that generates copper nanoparticles (NPs) on a silica support while simultaneously passivating the silica surface with trimethylsiloxy groups. The material is active for the catalytic semihydrogenation of phenylalkyl-, dialkyl- and diaryl-alkynes and displays high chemo- and stereoselectivity at full alkyne conversion to corresponding (Z)-olefins in the presence of an N-heterocyclic carbene (NHC) ligand. Solid-state NMR spectroscopy using the NHC ligand ^{13}C-labeled at the carbenic carbon reveals a genuine coordination of the carbene to Cu NPs. The presence of distinct Cu surface environments and the coordination of the NHC to specific Cu sites likely account for the increased selectivity.

Introduction

N-Heterocyclic carbenes (NHCs) belong to a class of prominent ligands, especially in homogeneous catalysis,[1–3] primarily due to their strong σ-donor properties[4] that yield organometallic complexes with very stable metal–carbon bonds.[2,5] NHC ligands have been utilized to improve the performance of numerous molecular catalysts in a broad range of applications such as olefin metathesis,[6] cross-coupling[7] and hydrogenation reactions,[8–10] to mention just a few. NHCs also bind to the surfaces of metallic nanoparticles (NPs) and wafers,[11–14] which was initially demonstrated for Au NPs[15,16] and recently exploited in catalytic applications,[17–21] such as electrocatalytic reduction of CO_2.[22,23] Another example is the use of Pd NPs decorated with NHC ligands for the Buchwald–Hartwig amination of aryl chlorides.[24]

Selective semihydrogenation of alkynes to alkenes is an important process used in both industry and academia.[25] The corresponding catalysts are typically based on Pd, among which the Lindlar catalyst[26] is most frequently used, even though it relies on scarce and expensive Pd metal and requires toxic Pb additive to achieve high selectivity. Copper-based materials are known to catalyze semihydrogenation of alkynes under flow conditions.[27,28] In this context, our group has recently reported that copper nanoparticles supported on a partially dehydroxylated silica

(Cu/SiO_{2-700}) efficiently catalyze batch semihydrogenation of alkynes in the presence of ligands (*e.g.* PCy_3)[29,30] with performances comparable to those of the Lindlar catalyst.[31] However, with certain substrates these earth-abundant Cu catalysts still display limited selectivity at full alkyne conversion due to the secondary hydrogenation of formed alkenes.

We reasoned that ligand functionalization of NPs[20,22–24,32–36] would improve chemoselectivity towards alkenes through competitive adsorption or poisoning of unselective sites by strong σ-donor ligands such as NHCs.[29] However, free NHCs are strong bases (imidazolium-/-ylidene couples typically have pK_a values in the 20–29 range)[37,38] and as such deprotonate the surface silanols of silica. In order to favor the selective coordination of an NHC ligand on the Cu sites, we use Surface Organometallic Chemistry (SOMC)[39] with a tailored molecular precursor, $[Cu_4(HMDS)_4]$ (HMDS = $N(SiMe_3)_2$) to synthesize Cu nanoparticles on passivated silica (that is silica where surface silanols are replaced by trimethylsilyloxy groups, SiO_{2-TMS}).[40,41] The resulting material (Cu/SiO_{2-TMS}) is a highly active alkyne hydrogenation catalyst that becomes selective towards semihydrogenation by addition of a prototypical NHC ligand, IMes (IMes = 1,3-bis(2,4,6-trimethylphenyl)imidazol-2-ylidene),[42] through the binding of IMes to mostly Cu surface sites as revealed by solid-state NMR spectroscopy.

Results and discussion

Preparation of Cu/SiO$_{2-TMS}$

The SOMC approach exploits the reactivity of $[Cu_4(HMDS)_4]$ that was prepared on the gram scale from $[Cu_2(COD)_2Cl_2]$[43] (COD = 1,5-cyclooctadiene) and NaHMDS (39% yield, see ESI† for details).[44] This Cu precursor reacts with SiO_{2-700} (2.1 equiv. Cu

ETH Zürich, Department of Chemistry and Applied Biosciences, Vladimir-Prelog-Weg 1-5, CH-8093, Zürich, Switzerland. E-mail: fedoroal@ethz.ch; ccoperet@ethz.ch

per surface ≡Si–OH site) in THF at 60 °C (Scheme 1) to yield a material containing 2.12, 1.81, 0.29 and 0.26 wt% loadings of Cu, C, H and N, respectively, by elemental analysis.

IR spectroscopy (Fig. 1) reveals that isolated silanols are fully consumed when $[Cu_4(HMDS)_4]$ is contacted with SiO_{2-700} (disappearance of the sharp band at 3747 cm^{-1} with concomitant appearance of C–H stretching bands at 2902 and 2954 cm^{-1} associated with SiMe$_3$ groups). The ^{1}H, ^{13}C and ^{29}Si solid-state NMR spectra of the grafted material indicate the presence of SiMe$_3$ groups in two different chemical environments (^{1}H: 0.8 and 0.5 ppm, ^{13}C: 7 and 0 ppm and ^{29}Si: 2 and 15 ppm, Fig. S1†) corresponding to N(SiMe$_3$)$_2$ and OSiMe$_3$, respectively.[40]
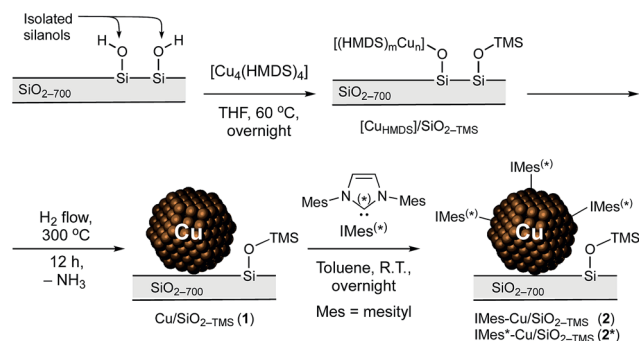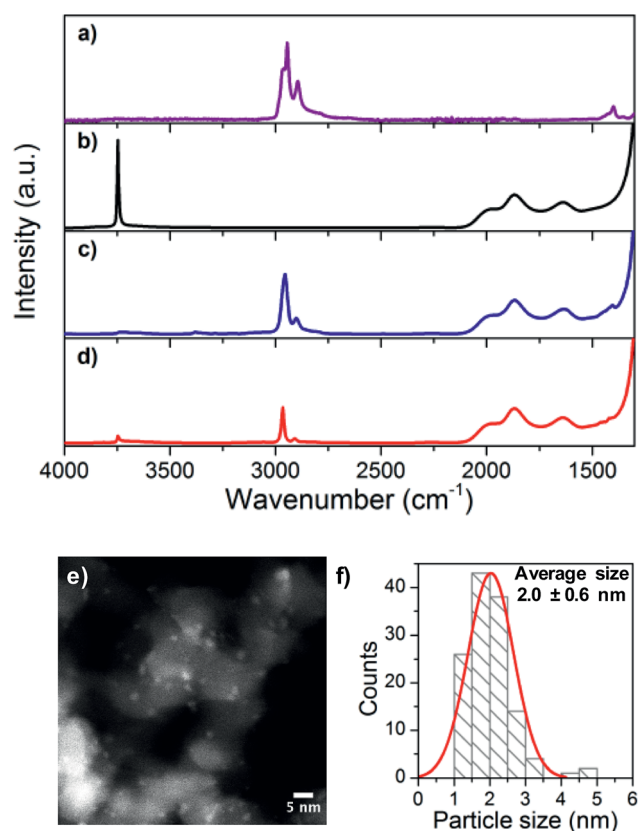

Scheme 1 Synthetic route to 1 and 2.

Fig. 1 FT-IR spectra of (a) $[Cu_4(HMDS)_4]$, (b) SiO_{2-700}, (c) $[Cu_{HMDS}]$/SiO_{2-TMS}, and (d) Cu/SiO_{2-TMS} (1) and (e) HR-TEM image and (f) particle size distribution of 1.

These observations are consistent with the formation of isolated multinuclear Cu along with ≡Si–OSiMe$_3$ surface sites by grafting of $[Cu_4(HMDS)_4]$ on SiO_{2-700} via protonolysis, releasing HN(TMS)$_2$ that further passivates remaining free silanols[40,41] ($[Cu_{HMDS}]$/SiO_{2-TMS}, Scheme 1). Treatment of $[Cu_{HMDS}]$/SiO_{2-TMS} under a flow of H$_2$ at 300 °C results in a color change from white to dark red and affords Cu/SiO_{2-TMS} (1). The HR-TEM images of 1 show the presence of small, well dispersed Cu NPs with a narrow size distribution of 2.0 ± 0.6 nm (Fig. 1e and f). Elemental analysis of 1 indicates a Cu loading of 2.31 wt%, and H$_2$ chemisorption gives ca. 0.07 mmol Cu$_{surface}$ g^{-1} in Cu surface sites (Fig. S2†). This loading is lower compared to that obtained using the $[Cu_5(Mes)_5]$ precursor (5.5 wt%, 0.31 mmol Cu$_{surface}$ g^{-1}),[29] in agreement with the competing passivation of silanol sites by Me$_3$Si groups that consequently limits the density of Cu sites upon grafting.

The IR spectrum of 1 displays a strong C–H stretching band at 2967 cm^{-1}, along with a weak band at 3747 cm^{-1} that is associated with the presence of a small amount of residual ≡Si–OH sites (ca. 10% with respect to initial silanols, Fig. 1d). NMR analysis (Fig. S1†) shows that 1 features a single set of peaks at 0.5 ppm (^{1}H), 0 ppm (^{13}C) and 15 ppm (^{29}Si), pointing to a single chemical environment for SiMe$_3$ groups. These observations are consistent with the formation of Cu NPs from ≡Si–O–[Cu$_n$(HMDS)$_m$] sites upon H$_2$ treatment, regenerating surface silanols that are mostly directly passivated into ≡Si–O–SiMe$_3$ sites by released HN(SiMe$_3$)$_2$.

Activity in alkyne hydrogenation

Next, we recorded H$_2$ consumption profiles during hydrogenation of a prototypical substrate 1-phenyl-1-propyne (S1) catalyzed by 1 (20 bar H$_2$, 60 °C, 1.8 mol% Cu$_{total}$, 0.4 mol% Cu$_{surface}$), both with or without additional ligands in the reaction media (Fig. 2). Two subsequent linear trends are observed in the H$_2$ consumption profile for the unmodified catalyst 1 (Fig. 2c, black trace). The first linear slope of ca. 4.3×10^{-2} mol H$_2$ L^{-1} h^{-1} (1.2×10^{-5} mol H$_2$ L^{-1} s^{-1}) at early stages is associated with hydrogenation of S1 to the (Z)-S1$_{2H}$. Following the full hydrogenation to S1$_{2H}$, the overhydrogenation of S1$_{2H}$ to S1$_{4H}$ occurs at a faster rate (second, steeper linear slope) of ca. 1.8×10^{-1} mol H$_2$ L^{-1} h^{-1} (5.0×10^{-5} mol H$_2$ L^{-1} s^{-1}). GC analysis of the reaction mixture after 16 h confirms quantitative conversion of S1 to S1$_{4H}$ (Fig. 2c, black, and Table 1, entry 1). The two-step behavior of the process likely originates from inhibition of the overhydrogenation by the starting alkyne until the latter gets depleted, and only then formation of S1$_{4H}$ proceeds. The fast rate of overhydrogenation at high conversion is thus responsible for the quick deterioration of chemoselectivity in the desired cis-olefinic product.

Introducing 2 mol% of IMes (ca. 1 : 6 Cu$_{surface}$/IMes ratio) to the catalytic mixture does not significantly change the initial rate of hydrogenation of 1-phenyl-1-propyne, as follows from a very similar slope in the H$_2$ uptake profile (5.0×10^{-2} mol H$_2$ L^{-1} h^{-1} and 1.4×10^{-5} mol H$_2$ L^{-1} s^{-1}; Fig. 2c, red trace). These unaltered rates suggest no poisoning of catalytic sites by IMes binding. However, the overhydrogenation to S1$_{4H}$ is fully
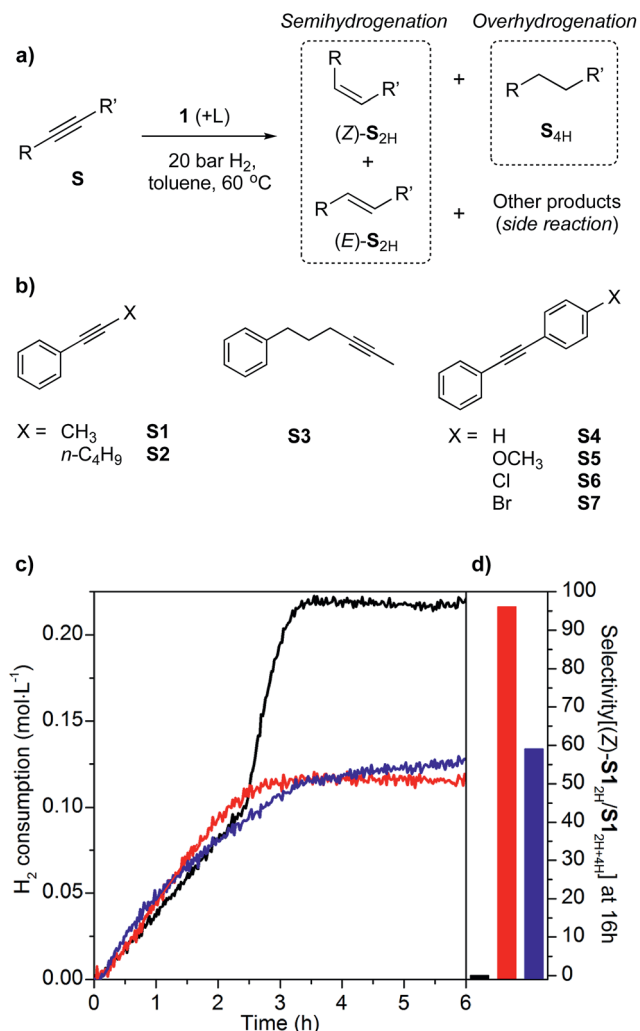
Fig. 2 Hydrogenation of alkynes with catalyst 1: (a) General reaction scheme, (b) substrate scope, (c) H_2 consumption profiles for hydrogenation of 1-phenyl-1-propyne ($S1$, 400 μmol) at 20 bar, 60 °C in toluene over unmodified 1 (black, 1.8 mol% Cu_{total}) or in the presence of IMes (red) or PCy_3 (blue) using a ligand/$S1$ molar ratio of 1 : 50, and (d) selectivity to (Z)-$S1_{2H}$ among hydrogenation products $S1_{2H}$ and $S1_{4H}$ (selectivity[(Z)-$S1_{2H}/S1_{2H+4H}$]) at the final time (16 h).

Table 1 Selectivities among hydrogenation products ($S1_{2H}$ and $S1_{4H}$) for the hydrogenation of $S1$ (20 bar, 60 °C, 16 h) with catalyst 1 at 1.8 mol% Cu_{total} loading. All reactions lead to complete conversion (>99%) of $S1$

Entry	Ligand	L/$S1$ ratio	Sel. $S1_{2H}$ (Z/E) (%)	Sel. $S1_{4H}$ (%)
1	—	—	<1	>99
2	IMes	1 : 50	97 (99 : 1)	3
3	IMes	1 : 100	95 (98 : 2)	5
4	IMes	1 : 500	12 (58 : 42)	88
5	PCy_3	1 : 50	66 (89 : 11)	34

inhibited in the presence of IMes and the chemoselectivity to (Z)-$S1_{2H}$ remains at 97% even after 16 h of reaction (Fig. 2c, red, and Table 1, entry 2). The high (Z)-$S1_{2H}$ chemoselectivity is also retained at a lower IMes/$S1$ ratio of 1 : 100 (Table 1, entry 3 and

Fig. S3†). Furthermore, GC analysis using an internal standard reveals only minor amounts of unidentified side products (1%, Table S1,† entry 2), possibly oligomers, confirming the very high overall selectivity to (Z)-$S1_{2H}$ with added IMes.

Hot filtration experiments showed no further conversion of $S1$ after removal of catalysts from the reaction mixture with or without added IMes, thereby demonstrating that no leaching of copper occurs, consistent with our previous observations.[29]

Control experiments reveal that while (Z)-$S1_{2H}$ is readily hydrogenated by 1, introducing IMes (2 mol% with respect to (Z)-$S1_{2H}$) completely shuts down the conversion of the alkene (Table S2†). This result clearly demonstrates that the NHC ligand inhibits hydrogenation of (Z)-$S1_{2H}$ to $S1_{4H}$, thereby avoiding overhydrogenation. For comparison, when IMes is replaced by tricyclohexylphosphine (2 mol% PCy_3), over-hydrogenation is not completely hindered, thus compromising the selectivity, in particular at high conversion (Fig. 2c and d, blue traces, and Tables 1, entry 5, and S2†).

To illustrate that IMes generally improves selectivity for semihydrogenation, we submitted several additional phenyl-alkyl-, dialkyl- and diarylalkynes[45] ($S2$–$S7$, Fig. 2b) to hydrogenation over 1 with or without added IMes. We optimized conditions (1 : 50 IMes/substrate ratio, 20 bar, 60 °C, 24 h, 9 mol% Cu_{total}, 2 mol% $Cu_{surface}$) to ensure full conversion of the starting alkyne, which was successfully achieved for all substrates except $S7$ (vide infra, Table 2). At this extended reaction time and significantly higher catalyst loading, $S1$ retains good selectivity to $S1_{2H}$ (88%) in the presence of IMes that is however completely lost due to $S1_{4H}$ (>99%) when IMes is not added (Table 2, entries 1–2). Being structurally related to $S1$, 1-phenyl-1-hexyne ($S2$) likewise displays high selectivity for semihydrogenation to $S2_{2H}$ (91%) only in the presence of IMes, whereas complete overhydrogenation to the corresponding alkane is observed using pristine 1; both reactions proceed without detected side-products (Table 2, entries 3–4). The selectivity to the (Z)-olefin is very high for the aliphatic alkyne $S3$ (99% to $S3_{2H}$, >99 : 1 Z/E ratio) when IMes is added to the reaction mixture, in contrast to what is observed in the absence of the ligand, where lower Z selectivity ($Z/E = 91 : 9$) and substantial by-product formation occur (17%), presumably due to oligomerization (Table 2, entries 5–6).

The semihydrogenation of diphenylacetylenes $S4$ and $S5$ in the presence of IMes provides respective (Z)-olefins in very high yields (>96%); in contrast, complete overhydrogenation to the corresponding diphenylethanes occurs when IMes is not added (>99% selectivity, Table 2, entries 7–10). The chloro-derivative $S6$ yields mostly $S6_{4H}$ (72% selectivity) over the unmodified catalyst 1 while $S6_{2H}$ is obtained with 28% selectivity. Interestingly, $S6_{2H}$ formed with pristine 1 is roughly an equal mixture of Z- and E-isomers (Table 2, entry 11). Addition of the IMes ligand alleviates low chemo- and stereoselectivities, yielding Z-stilbene $S6_{2H}$ in 93% yield (Table 2, entry 12). The bromo-derivative $S7$ does not reach full conversion both with or without added IMes (66 and 79% conversion, respectively) and features high selectivity to (Z)-$S7_{2H}$ in both cases (>99%, entries 13–14). This high chemoselectivity to (Z)-$S7_{2H}$ likely originates from the remaining alkyne $S7$, consistent with the inhibition of the

Table 2 Conversions and overall selectivities for hydrogenation (20 bar, 60 °C, 24 h) with catalyst **1** (9 mol% Cu_{total}) in the presence or absence of IMes using a IMes/substrate molar ratio of 1 : 50 (see ESI for details)

Entry	Substrate	Ligand	Conv. (%)	Sel. S_{2H} (%)	S_{2H} Z/E ratio	Sel. others (S_{4H}) (%)
1	**S1**	—	>99	<1	—	>99 (>99)
2	**S1**	IMes	>99	88	90 : 10	<1 (—)
3	**S2**	—	>99	<1	—	>99 (>99)
4	**S2**	IMes	>99	91	91 : 9	9 (9)
5	**S3**	—	>99	83	91 : 9	17 (<1)^a
6	**S3**	IMes	>99	99	>99 : 1	1 (<1)^a
7	**S4**	—	>99	<1	—	>99 (>99)
8	**S4**	IMes	>99	>99	97 : 3	<1 (—)
9	**S5**	—	>99	<1	—	>99 (>99)
10	**S5**	IMes	>99	>99	97 : 3	<1 (—)
11	**S6**	—	>99	28	48 : 52	72 (72)
12	**S6**	IMes	>99	96	98 : 2	4 (4)
13	**S7**	—	79	>99	99 : 1	<1
14	**S7**	IMes	66	>99	99 : 1	<1

^{a} Mass balance indicates the formation of undetected side products, likely oligomers.

overhydrogenation by the starting alkyne, as was also reported previously.[29] We note that both halogen-containing substrates **S6** and **S7** react slower over catalyst **1**, possibly due to the interaction of the Cu surface with the halogen substituent. The latter effect would also be consistent with the high fraction of a chloro-stilbene (E)-**S6**$_{2H}$ formed with pristine catalyst **1**, probably through a secondary isomerization of (Z)-**S6**$_{2H}$ on a Cu surface that had possibly been modified by an interaction with the Cl-substituent (Table 2, entry 11). Overall, these results demonstrate that the enhancement in selectivity provided by IMes can be extended to phenylalkyl, dialkyl and diaryl internal alkynes. These findings further underline the impressive effect of IMes on inhibiting the undesired overhydrogenation of internal olefins and also hindering side reactions such as oligomerization and olefin isomerization, especially at elevated temperature (60 °C).[29]

Characterizing the ligand–particle interaction

To understand the origin of the improved chemoselectivity, we studied the nature of the IMes–Cu NP interaction at the molecular level using solid-state NMR. Contacting **1** with a toluene solution of IMes*, ^{13}C-labeled at the carbenic carbon, followed by washing of the resulting material with toluene and pentane and drying under vacuum yields IMes*–Cu/SiO$_{2-TMS}$ (**2***, the labeled analogue of **2**, Scheme 1). Elemental analysis of **2*** gives 1.82, 3.37, 0.48 and 0.44 wt% Cu, C, H and N, respectively, consistent with the immobilization of IMes* on Cu/SiO$_{2-TMS}$ (Table S3†). Elemental analysis data allow estimating the Cu$_{surface}$/IMes ratio to be *ca.* 1 : 1.4, suggesting concomitant binding of IMes* on both Cu NPs and the support. The IR spectrum of **2** contains bands reminiscent of the NHC ligand, confirming adsorption of IMes onto **1** (Fig. S4†). Exposure of **1** to 33 mbar of CO (Fig. S5†) gives a broad IR band between 2000–2200 cm^{-1} that can be decomposed into 3 main components centered at 2119, 2095 and 2055 cm^{-1}. Repeating the experiment with **2** (Fig. S5†) produces CO bands that are less intense, possibly because its adsorption is hindered by

the bulky NHC ligand, as already observed with PCy$_3$-functionalized non-passivated Cu/SiO$_{2-700}$.[29] Moreover, the feature at 2119 cm^{-1} disappears whereas a new band appears at 2004 cm^{-1}, resulting in an overall red shift of CO adsorption modes. This red shift points to a stronger back-donation to CO, consistent with more electron-rich Cu NPs as expected from binding of an IMes ligand to the Cu surface. Furthermore, X-ray absorption near edge structure (XANES) spectroscopy of **1** and **2** demonstrates a slight change in the Cu-K white line from 8996.5 to 8996.7 eV that also supports binding of IMes on Cu NPs (Fig. S6†).

NMR spectroscopy is particularly instrumental in elucidating the coordination of ligands, including NHCs, on transition-metal NPs.[18,19,22,24,46–48] The ^{13}C direct excitation spectrum of **2*** (Fig. 3b) reveals a major, broad peak centered at 178 ppm and a shoulder at 189 ppm, which are also present in the ^{13}C cross-polarization (CP) spectrum (Fig. 3c). In contrast, these peaks disappear in the ^{13}C CP spectrum of **2** (Fig. 3e) and can thus be attributed to ^{13}C-labeled carbons in **2***. In addition, the intensity of the peak at 178 ppm relative to that of TMS groups of the support (−2 ppm) increases in the direct excitation spectrum compared to the CP one (Fig. S7b and c†), pointing to carbon atoms not directly bonded to protons. With these observations, we assign the peak at 178 ppm to (^{13}C-labeled) carbenic carbons coordinated to Cu NPs. This assignment is further supported by the upfield shift of this peak compared to the carbenic carbon in free IMes* (219 ppm, Fig. 3a)[49] and by the similarity of the observed shifts to values reported for NHC bound to Cu sites in [Cu(IMes)(L)] molecular complexes.[50] In the same ppm range, the shoulder at 189 ppm is also attributed to Cu-bound carbenic carbons, likely in a different environment. The relative intensity of this peak is similar in the direct excitation and CP spectra (Fig. S7b and c†), suggesting the presence of protons in the vicinity of the carbene ligand, possibly associated with Cu sites closer to the interface with the SiO$_{2-TMS}$ support. Alternative interpretations are that distinct resonances at 178 and 189 ppm arise from IMes bound
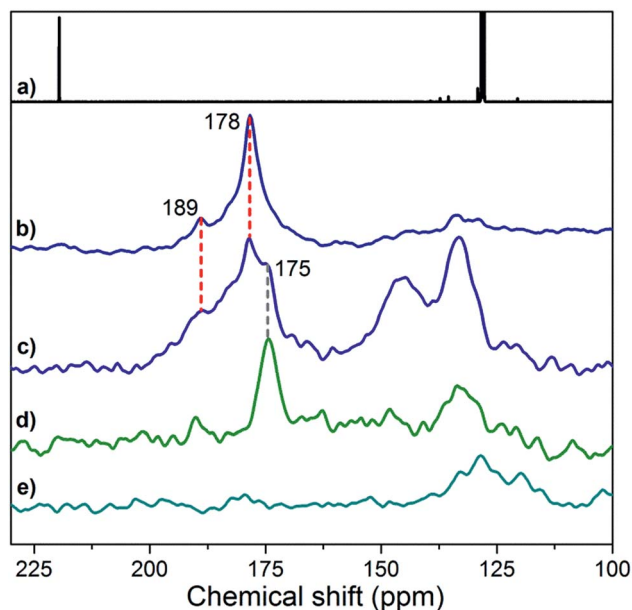
Fig. 3 (a) ^{13}C NMR solution-state spectrum of free IMes* (C_6D_6, 75 MHz); (b) ^{13}C NMR solid-state HPDEC spectrum of **2*** (30 000 scans); ^{13}C NMR solid-state CP-MAS spectra of (c) **2*** (90 000 scans), (d) IMes*/SiO$_{2\text{-TMS}}$ (27 513 scans) and (e) **2** (90 000 scans). Broader spectral windows are provided in Fig. S7 and S8† and ^{1}H NMR spectra for IMes* and **2*** are given in Fig. S9.†

on (111) and (200) facets, which are expected to be present on Cu nanoparticles,[51] or from high (terraces) and low (corners or edges) coordination sites present on Cu NPs.

The peak at 175 ppm in the CP spectrum of **2*** (Fig. 3c) is attributed to the ^{13}C-labeled carbenic carbon of IMes* in interaction with the support, as this peak is also found for the fully passivated SiO$_{2\text{-TMS}}$ support contacted with IMes* (IMes*/SiO$_{2\text{-TMS}}$, Fig. 3d and S7e†) and it may be due to the carbene coordinated to Si atoms[52] in TMS groups or siloxane bridges. Peaks at 133 and 145 ppm in the CP spectrum of **2*** (Fig. 3c) are also observed for non-passivated SiO$_{2\text{-700}}$ treated with IMes* (Fig. S7f†); they are assigned to ^{13}C-labeled imidazolium species formed on the support upon deprotonation of residual silanols by IMes*. The observation of peaks attributed to surface species on the support itself is also consistent with elemental analysis of **2***, which shows the presence of an excess of the ligand per available surface Cu atom.

Collectively, these results prove the immobilization of IMes in **2*** with a partial coverage of the support and actual ligand–particle interaction through genuine coordination of the carbenic carbon to the copper particle.

Conclusion

In conclusion, we report the controlled synthesis of small Cu NPs supported on Me$_3$Si-passivated SiO$_{2\text{-700}}$ through SOMC. The supported Cu NPs are highly active for the hydrogenation of alkynes, and introduction of an NHC ligand greatly improves the selectivity of these particles for semihydrogenation of phenylalkyl, dialkyl and diaryl internal alkynes generating the

corresponding *cis*-olefins with very high selectivities (>95%) at full conversion. This increased selectivity likely arises from the binding of the IMes ligand to Cu NPs, in a genuine coordination which has been confirmed by ^{13}C NMR spectroscopy. This work shows that inexpensive and readily available supported Cu nanoparticles can be turned into highly selective catalysts by choosing appropriate coordinating ligands to modulate their activity and selectivity. Our group is currently exploring this research direction.

Conflicts of interest

There are no conflicts to declare.

Acknowledgements

Notes and references

1 J. C. Lin, R. T. Huang, C. S. Lee, A. Bhattacharyya, W. S. Hwang and I. J. Lin, *Chem. Rev.*, 2009, **109**, 3561–3598.
2 C. M. Crudden and D. P. Allen, *Coord. Chem. Rev.*, 2004, **248**, 2247–2273.
3 M. N. Hopkinson, C. Richter, M. Schedler and F. Glorius, *Nature*, 2014, **510**, 485–496.
4 T. Dröge and F. Glorius, *Angew. Chem., Int. Ed.*, 2010, **49**, 6940–6952.
5 W. A. Herrmann and C. Köcher, *Angew. Chem., Int. Ed. Engl.*, 1997, **36**, 2162–2187.
6 G. C. Vougioukalakis and R. H. Grubbs, *Chem. Rev.*, 2010, **110**, 1746–1787.
7 R. D. J. Froese, C. Lombardi, M. Pompeo, R. P. Rucker and M. G. Organ, *Acc. Chem. Res.*, 2017, **50**, 2244–2253.
8 E. Peris and R. H. Crabtree, *Coord. Chem. Rev.*, 2004, **248**, 2239–2246.
9 D. Zhao, L. Candish, D. Paul and F. Glorius, *ACS Catal.*, 2016, **6**, 5978–5988.
10 J. W. Sprengers, J. Wassenaar, N. D. Clement, K. J. Cavell and C. J. Elsevier, *Angew. Chem., Int. Ed.*, 2005, **44**, 2026–2029.
11 A. V. Zhukhovitskiy, M. J. MacLeod and J. A. Johnson, *Chem. Rev.*, 2015, **115**, 11503–11532.
12 K. Salorinne, R. W. Y. Man, C. H. Li, M. Taki, M. Nambo and C. M. Crudden, *Angew. Chem., Int. Ed.*, 2017, **56**, 6198–6202.

13 C. M. Crudden, J. H. Horton, I. I. Ebralidze, O. V. Zenkina, A. B. McLean, B. Drevniok, Z. She, H. B. Kraatz, N. J. Mosey, T. Seki, E. C. Keske, J. D. Leake, A. Rousina-Webb and G. Wu, *Nat. Chem.*, 2014, **6**, 409–414.

14 G. Wang, A. Ruhling, S. Amirjalayer, M. Knor, J. B. Ernst, C. Richter, H. J. Gao, A. Timmer, H. Y. Gao, N. L. Doltsinis, F. Glorius and H. Fuchs, *Nat. Chem.*, 2017, **9**, 152–156.

15 J. Vignolle and T. D. Tilley, *Chem. Commun.*, 2009, 7230–7232.

16 E. C. Hurst, K. Wilson, I. J. S. Fairlamb and V. Chechik, *New J. Chem.*, 2009, **33**, 1837.

17 C. Richter, K. Schaepe, F. Glorius and B. J. Ravoo, *Chem. Commun.*, 2014, **50**, 3204–3207.

18 L. M. Martinez-Prieto, A. Ferry, L. Rakers, C. Richter, P. Lecante, K. Philippot, B. Chaudret and F. Glorius, *Chem. Commun.*, 2016, **52**, 4768–4771.

19 J. B. Ernst, S. Muratsugu, F. Wang, M. Tada and F. Glorius, *J. Am. Chem. Soc.*, 2016, **138**, 10718–10721.

20 F. Novio, D. Monahan, Y. Coppel, G. Antorrena, P. Lecante, K. Philippot and B. Chaudret, *Chem. –Eur. J.*, 2014, **20**, 1287–1297.

21 K. V. Ranganath, J. Kloesges, A. H. Schafer and F. Glorius, *Angew. Chem., Int. Ed.*, 2010, **49**, 7786–7789.

22 Z. Cao, D. Kim, D. Hong, Y. Yu, J. Xu, S. Lin, X. Wen, E. M. Nichols, K. Jeong, J. A. Reimer, P. Yang and C. J. Chang, *J. Am. Chem. Soc.*, 2016, **138**, 8120–8125.

23 Z. Cao, J. S. Derrick, J. Xu, R. Gao, M. Gong, E. M. Nichols, P. T. Smith, X. Liu, X. Wen, C. Copéret and C. J. Chang, *Angew. Chem., Int. Ed.*, 2018, **57**, 4981–4985.

24 J. B. Ernst, C. Schwermann, G. I. Yokota, M. Tada, S. Muratsugu, N. L. Doltsinis and F. Glorius, *J. Am. Chem. Soc.*, 2017, **139**, 9144–9147.

25 G. Vilé, D. Albani, N. Almora-Barrios, N. López and J. Pérez-Ramírez, *ChemCatChem*, 2016, **8**, 21–33.

26 H. Lindlar, *Helv. Chim. Acta*, 1952, **35**, 446–450.

27 B. Bridier, M. A. G. Hevia, N. López and J. Pérez-Ramírez, *J. Catal.*, 2011, **278**, 167–172.

28 R. A. Koeppel, J. T. Wehrli, M. S. Wainwright, D. L. Trimma and N. W. Cant, *Appl. Catal., A*, 1994, **120**, 163–177.

29 A. Fedorov, H. J. Liu, H. K. Lo and C. Copéret, *J. Am. Chem. Soc.*, 2016, **138**, 16502–16507.

30 O. G. Salnikov, H. J. Liu, A. Fedorov, D. B. Burueva, K. V. Kovtunov, C. Copéret and I. V. Koptyug, *Chem. Sci.*, 2017, **8**, 2426–2430.

31 C. Oger, L. Balas, T. Durand and J. M. Galano, *Chem. Rev.*, 2013, **113**, 1313–1350.

32 I. Schrader, S. Neumann, A. Šulce, F. Schmidt, V. Azov and S. Kunz, *ACS Catal.*, 2017, **7**, 3979–3987.

33 I. Schrader, S. Neumann, R. Himstedt, A. Zana, J. Warneke and S. Kunz, *Chem. Commun.*, 2015, **51**, 16221–16224.

34 F. Zaera, *ACS Catal.*, 2017, **7**, 4947–4967.

35 S. Kunz, *Top. Catal.*, 2016, **59**, 1671–1685.

36 J. L. Castelbou, A. Gual, E. Mercadé, C. Claver and C. Godard, *Catal. Sci. Technol.*, 2013, **3**, 2828.

37 R. S. Massey, C. J. Collett, A. G. Lindsay, A. D. Smith and A. C. O'Donoghue, *J. Am. Chem. Soc.*, 2012, **134**, 20421–20432.

38 E. M. Higgins, J. A. Sherwood, A. G. Lindsay, J. Armstrong, R. S. Massey, R. W. Alder and A. C. O'Donoghue, *Chem. Commun.*, 2011, **47**, 1559–1561.

39 C. Copéret, A. Comas-Vives, M. P. Conley, D. P. Estes, A. Fedorov, V. Mougel, H. Nagae, F. Nunez-Zarur and P. A. Zhizhko, *Chem. Rev.*, 2016, **116**, 323–421.

40 E. Oakton, G. Vile, D. S. Levine, E. Zocher, D. Baudouin, J. Perez-Ramirez and C. Copéret, *Dalton Trans.*, 2014, **43**, 15138–15142.

41 D. Gajan, K. Guillois, P. Delichere, J. M. Basset, J. P. Candy, V. Caps, C. Copéret, A. Lesage and L. Emsley, *J. Am. Chem. Soc.*, 2009, **131**, 14667–14669.

42 A. J. Arduengo, H. V. R. Dias, R. L. Harlow and M. Kline, *J. Am. Chem. Soc.*, 1992, **114**, 5530–5534.

43 K. M. Chi, H. K. Shin, M. J. Hampden-Smith, E. N. Duesler and T. T. Kodas, *Polyhedron*, 1991, **10**, 2293–2299.

44 A. M. James, R. K. Laxman, F. R. Fronczek and A. W. Maverick, *Inorg. Chem.*, 1998, **37**, 3785–3791.

45 F. Chen, C. Kreyenschulte, J. Radnik, H. Lund, A.-E. Surkus, K. Junge and M. Beller, *ACS Catal.*, 2017, **7**, 1526–1532.

46 J. M. Asensio, S. Tricard, Y. Coppel, R. Andres, B. Chaudret and E. de Jesus, *Angew. Chem., Int. Ed.*, 2017, **56**, 865–869.

47 P. Lara, L. M. Martínez-Prieto, M. Roselló-Merino, C. Richter, F. Glorius, S. Conejero, K. Philippot and B. Chaudret, *Nano-Struct. Nano-Objects*, 2016, **6**, 39–45.

48 P. Lara, O. Rivada-Wheelaghan, S. Conejero, R. Poteau, K. Philippot and B. Chaudret, *Angew. Chem., Int. Ed.*, 2011, **50**, 12080–12084.

49 D. Tapu, D. A. Dixon and C. Roe, *Chem. Rev.*, 2009, **109**, 3385–3407.

50 O. Santoro, A. Collado, A. M. Slawin, S. P. Nolan and C. S. Cazin, *Chem. Commun.*, 2013, **49**, 10483–10485.

51 K. Larmier, S. Tada, A. Comas-Vives and C. Copéret, *J. Phys. Chem. Lett.*, 2016, **7**, 3259–3263.

52 F. Bonnette, T. Kato, M. Destarac, G. Mignani, F. P. Cossio and A. Baceiredo, *Angew. Chem., Int. Ed.*, 2007, **46**, 8632–8635.